aerospace

MDPI

Article

Optimal Circle-to-Ellipse Orbit Transfer for Sun-Facing E-Sail

Alessandro A. Quarta *, Giovanni Mengali, Marco Bassetto and Lorenzo Niccolai

Department of Civil and Industrial Engineering, University of Pisa, I-56122 Pisa, Italy
* Correspondence: a.quarta@ing.unipi.it

Abstract: The transfer between two coplanar Keplerian orbits of a spacecraft with a continuous-thrust propulsion system is a classical problem of astrodynamics, in which a numerical procedure is usually employed to find the transfer trajectory that optimizes (i.e., maximizes or minimizes) a given performance index such as, for example, the delivered payload mass, the propellant mass, the total flight time, or a suitable combination of them. In the last decade, this class of problem has been thoroughly analyzed in the context of heliocentric mission scenarios of a spacecraft equipped with an Electric Solar Wind Sail as primary propulsion system. The aim of this paper is to further extend the existing related literature by analyzing the optimal transfer of an Electric Solar Wind Sail-based spacecraft with a Sun-facing attitude, a particular configuration in which the sail nominal plane is perpendicular to the Sun-spacecraft (i.e., radial) direction, so that the propulsion system is able to produce its maximum propulsive acceleration magnitude. The problem consists in transferring the spacecraft, which initially traces a heliocentric circular orbit, into an elliptic coplanar orbit of given eccentricity with a minimum-time trajectory. Using a classical indirect approach for trajectory optimization, the paper shows that a simplified version of the optimal control problem can be obtained by enforcing the typical transfer constraints. The numerical simulations show that the proposed approach is able to quantify the transfer performance in a parametric and general form, with a simple and efficient algorithm.

Keywords: Electric Solar Wind Sail; Sun-facing attitude; optimal transfer; heliocentric mission analysis

Citation: Quarta, A.A.; Mengali, G.; Bassetto, M.; Niccolai, L. Optimal Circle-to-Ellipse Orbit Transfer for Sun-Facing E-Sail. *Aerospace* **2022**, *9*, 671. https://doi.org/10.3390/aerospace9110671

Academic Editor: Andris Slavinskis

Received: 11 October 2022
Accepted: 27 October 2022
Published: 29 October 2022

1. Introduction

An Electric Solar Wind Sail (or E-sail) [1] is a propellantless device, conceived by Dr. Pekka Janhunen in 2004 [2], whose aim is to navigate the interplanetary space by extracting momentum from the stream of solar wind charged particles. When compared to more conventional propulsion systems, such as chemical or electric thrusters, an E-sail presents interesting peculiarities, including the capability of guaranteing long-lasting space missions or the possibility of conceiving new scenarios and innovative mission concepts.

A very promising class of potential applications for an E-sail consists in the exploration of the outer regions of the Solar System. In this regard, Janhunen et al. [3] analyzed an E-sail-based transfer towards Uranus, while a more ambitious objective is represented by an escape from the Solar System to reach the heliopause [4–7], the Sun's gravitational focus [8], or even other stellar systems [9]. Notably, such long transfers can be made faster if the E-sail approaches the Sun in the first phase of its transfer trajectory. Such a strategy, referred to as solar wind assist [5], allows the E-sail to exploit the increased thrust due to a higher plasma density to reach very high orbital speeds and reduce the total mission time.

Other innovative mission scenarios that could be performed by an E-sail include the maintenance of displaced non-Keplerian orbits [10], the generation of artificial equilibrium points in the restricted three-body problem [11], and the asteroid deflection by means of a kinetic impactor [12,13]. Finally, an E-sail could also be exploited for deep space transfers towards planets [14,15], comets [16], asteroids [17], or other targets in the Solar System [18].

Since the E-sail propulsive acceleration depends on the orientation of its nominal plane [19] (that is, the mean plane containing the sail conducting tethers), the attitude control problem of an E-sail is closely related to that of its orbital control [20–23]. According to some preliminary studies [24–27], the particular orientation in which the E-sail nominal plane is perpendicular to the Sun-spacecraft line, referred to as Sun-facing configuration, may be passively maintained when the E-sail has an axisymmetric shape. Because of this relative simplicity from the standpoint of attitude control, much effort has been dedicated to the mission analysis of a Sun-facing E-sail configuration [28,29]. The latter is useful, for example, for generating spiral trajectories [30] or to perform phasing maneuvers [31]. A Sun-facing attitude has also been investigated for devices based on photonic propulsion [32–35], such as solar sails [36] or Smart Dusts [37], to simulate time-optimal transfer trajectories [38], to obtain closed-form solutions to the equations of motion [39], and to calculate the performance requirements for the maintenance of an artificial equilibrium point in the restricted three-body problem [40,41].

This paper focuses on two-dimensional transfers between heliocentric Keplerian orbits using a Sun-facing E-sail. It is assumed that the spacecraft departs from a circular parking orbit with the aim of reaching a coplanar target orbit of given eccentricity. Orbit-to-orbit transfers are analyzed in an optimal framework, where the total flight time is minimized with an indirect approach [42–44]. The novelty of the paper is to apply the optimal control theory to the special but important case when the direction of the E-sail propulsive acceleration vector is aligned with the Sun-spacecraft line. The resulting simplification of the control problem due to the reduced form of the thrust vector model, allows some useful analytical results to be obtained in a compact and elegant form. In particular, a set of dimensionless state variables is used in the dynamical model to make the results independent of the radius of the initial orbit. A parametric study is conducted, in which the transfer time is obtained as a function of the final eccentricity and the E-sail performance level. The optimal control law is then applied to simulate some potential heliocentric mission scenarios, including mission towards planets close to the Earth (Mars and Venus), or more ambitious targets, such as Jupiter.

The remainder of the manuscript is structured as follows. Section 2 introduces the dynamical model of a spacecraft subject to the Sun's gravity and propelled by a Sun-facing E-sail. It also describes the procedure for trajectory optimization. Section 3 shows the results of the parametric analysis and analyzes some potential mission applications. The concluding section summarizes the main outcomes of the paper.

2. Problem Description

Consider a spacecraft that initially traces a heliocentric circular (parking) orbit of assigned radius r_0. The spacecraft primary propulsion system is an E-sail that, after the deployment at time $t_0 \triangleq 0$, is maintained in a Sun-facing condition, so that its propulsive acceleration vector $\boldsymbol{a}_p$ is given by the following compact equation

$$\boldsymbol{a}_p = s\,\beta\,\frac{\mu_\odot}{r_0^2}\left(\frac{r_0}{r}\right)\hat{\boldsymbol{\imath}}_r \equiv s\,\beta\,\frac{\mu_\odot}{r_0\,r}\hat{\boldsymbol{\imath}}_r \tag{1}$$

where $\mu_\odot$ is the Sun's gravitational parameter, r is the Sun-spacecraft distance, $\hat{\boldsymbol{\imath}}_r$ is the radial (or Sun-spacecraft) unit vector, and $s \in \{0, 1\}$ is a dimensionless switching parameter that models the E-sail electron gun on ($s = 1$) or off ($s = 0$) condition. Here, s is introduced to account for possible coasting arcs (obtained with $s = 0$) in the spacecraft heliocentric trajectory. In Equation (1), β is a dimensionless positive parameter, defined as the ratio of the maximum propulsive acceleration magnitude $\|\boldsymbol{a}_p\|$ to the Sun's gravitational acceleration along the parking orbit, when $r = r_0$. Note that β is a sort of reference propulsive acceleration, whose value depends on both the spacecraft mass and the E-sail design characteristics, such as the number and the length of the conducting tethers [45].

Using the propulsive acceleration of Equation (1) and assuming a simplified mission scenario where the external forces on the spacecraft are the E-sail thrust and the Sun's gravitational pull only, it is easily concluded that the spacecraft propelled trajectory belongs to the parking orbit plane, and the semilatus rectum p of the osculating orbit is a constant of motion, that is

$$p \equiv r_0 \qquad \text{for} \qquad t \geq t_0 \tag{2}$$

Accordingly, the Sun-facing E-sail can potentially reach an elliptic Keplerian (target) orbit of eccentricity $e_f < 1$ and semilatus rectum $p_f = r_0$, which is coplanar to the circular parking orbit. The aim of this paper is to analyze the optimal transfer trajectory that minimizes the flight time $\Delta t \triangleq t_f - t_0 \equiv t_f$ necessary for the E-sail to obtain a rendez-vous with a target coplanar orbit of given eccentricity e_f. In particular, the orientation of the target orbit apse line (measured with respect to the Sun-spacecraft line at time t_0) is left free and is an output of the optimization process described at the end of this section.

2.1. Spacecraft Dynamics

The two-dimensional spacecraft dynamics can be studied by introducing a heliocentric polar reference frame $\mathcal{T}(O; \hat{\boldsymbol{i}}_r, \hat{\boldsymbol{i}}_\theta)$, whose origin coincides with the Sun's center of mass O, where $\hat{\boldsymbol{i}}_\theta$ is the transverse (or circumferential) unit vector in the direction of the spacecraft inertial velocity; see Figure 1.

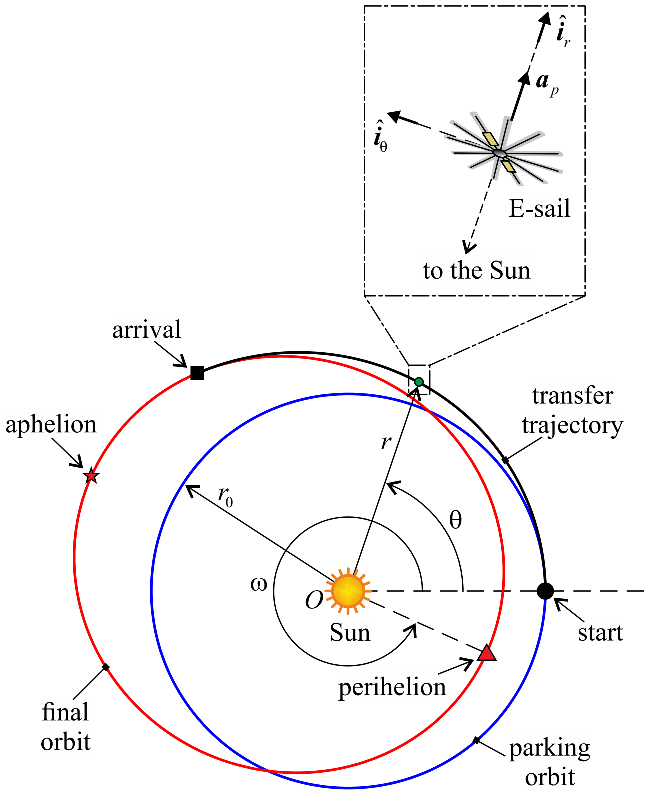

Figure 1. Reference frame and E-sail-based spacecraft state variables.

Bearing in mind that the semilatus rectum of the osculating orbit is a constant of motion and using Equation (1) for the propulsive acceleration vector, the spacecraft equations of motion in the polar reference frame are

$$\frac{\mathrm{d}r}{\mathrm{d}t} = u \tag{3}$$

$$\frac{\mathrm{d}\theta}{\mathrm{d}t} = \frac{h}{r^2} \equiv \frac{\sqrt{\mu_\odot\, r_0}}{r^2} \tag{4}$$

$$\frac{\mathrm{d}u}{\mathrm{d}t} = -\frac{\mu_\odot}{r^2} + \frac{h^2}{r^3} + s\,\beta\,\frac{\mu_\odot}{r_0^2}\left(\frac{r_0}{r}\right) \equiv \frac{\mu_\odot}{r^2}\left(-1 + \frac{r_0}{r} + s\,\beta\,\frac{r}{r_0}\right) \tag{5}$$

where u is the radial component of the spacecraft inertial velocity vector, θ is the polar angle measured counterclockwise from the initial Sun-spacecraft line (see Figure 1), and

$$h = \sqrt{\mu_\odot\, p} \equiv \sqrt{\mu_\odot\, r_0} \tag{6}$$

is the (constant) specific angular momentum of the spacecraft osculating orbit. The nonlinear differential Equations (3)–(5) are completed by the following initial conditions

$$r(t_0) = r_0 \quad , \quad \theta(t_0) = 0 \quad , \quad u(t_0) = 0 \tag{7}$$

where, without loss of generality, it is assumed that the initial spacecraft polar angle is zero. The spacecraft dynamics can be more conveniently described in a dimensionless form by introducing the auxiliary (dimensionless) variables

$$\tau \triangleq t\,\sqrt{\frac{\mu_\odot}{r_0^3}} \quad , \quad \rho \triangleq \frac{r}{r_0} \quad , \quad v \triangleq u\,\sqrt{\frac{r_0}{\mu_\odot}} \tag{8}$$

so that the equations of motion (3)–(5) can be rewritten as

$$\frac{\mathrm{d}\rho}{\mathrm{d}\tau} = v \tag{9}$$

$$\frac{\mathrm{d}\theta}{\mathrm{d}\tau} = \frac{1}{\rho^2} \tag{10}$$

$$\frac{\mathrm{d}v}{\mathrm{d}\tau} = -\frac{1}{\rho^2} + \frac{1}{\rho^3} + \frac{s\,\beta}{\rho} \tag{11}$$

while the initial conditions (7) become

$$\rho(\tau_0) = 1 \quad , \quad \theta(\tau_0) = 0 \quad , \quad v(\tau_0) = 0 \tag{12}$$

where $\tau_0 \triangleq 0$ is the initial dimensionless time.

The τ-variation of the E-sail switching parameter s is chosen to minimize the flight time $\Delta\tau = \tau_f - \tau_0 \equiv \tau_f$ necessary for the spacecraft to reach an osculating elliptic orbit of given eccentricity $e_f < 1$. Note that this amounts to reaching a Keplerian orbit with a semimajor axis

$$a_f = \frac{r_0}{1 - e_f^2} \tag{13}$$

or a specific mechanical energy

$$E_f = -\frac{\mu_\odot}{2\,a_f} \equiv \frac{\mu_\odot\left(e_f^2 - 1\right)}{2\,r_0} \tag{14}$$

The latter relation, in a dimensionless form, becomes

$$\mathcal{E}_f \triangleq \frac{E_f}{\mu_\odot / r_0} = \frac{e_f^2 - 1}{2} \tag{15}$$

The optimal function $s = s(\tau)$, with $\tau \in [0,\, \tau_f]$, and the corresponding value of the minimum flight time τ_f are the solution of the minimum-time problem described in the next section.

2.2. Trajectory Optimization

The optimal transfer trajectory is obtained by maximizing the dimensionless performance index

$$J \triangleq -\tau_f \tag{16}$$

Using an indirect approach, introduce the Hamiltonian function

$$\mathcal{H} \triangleq \lambda_\rho \, v + \frac{\lambda_\theta}{\rho^2} + \lambda_v \left(-\frac{1}{\rho^2} + \frac{1}{\rho^3} + \frac{s\,\beta}{\rho} \right) \tag{17}$$

where $\{\lambda_\rho, \lambda_\theta, \lambda_v\}$ are the costates of $\{\rho, \theta, v\}$, respectively. The τ-variation of the costates is described by the Euler-Lagrange equations

$$\frac{\mathrm{d}\lambda_\rho}{\mathrm{d}\tau} \triangleq -\frac{\partial \mathcal{H}}{\partial \rho} = \frac{3\,\lambda_v}{\rho^4} - \frac{2\,\lambda_v}{\rho^3} + \frac{s\,\beta\,\lambda_v}{\rho^2} + \frac{2\,\lambda_\theta}{\rho^3} \tag{18}$$

$$\frac{\mathrm{d}\lambda_\theta}{\mathrm{d}\tau} \triangleq -\frac{\partial \mathcal{H}}{\partial \theta} = 0 \tag{19}$$

$$\frac{\mathrm{d}\lambda_v}{\mathrm{d}\tau} \triangleq -\frac{\partial \mathcal{H}}{\partial v} = -\lambda_\rho \tag{20}$$

In particular, Equation (19) states that λ_θ is a constant of motion, whose value is found by enforcing the transversality condition. In fact, assuming that the spacecraft final angular position θ_f is left free, the transversality condition on λ_θ is

$$\lambda_\theta = 0 \tag{21}$$

and Equation (18) becomes

$$\frac{\mathrm{d}\lambda_\rho}{\mathrm{d}\tau} = \frac{3\,\lambda_v}{\rho^4} - \frac{2\,\lambda_v}{\rho^3} + \frac{s\,\beta\,\lambda_v}{\rho^2} \tag{22}$$

Instead, the initial value of the costate λ_v is derived by exploiting the transversality condition on the final value of the Hamiltonian function, that is

$$\mathcal{H}(\tau_f) = 1 \tag{23}$$

Indeed, observing that $\mathcal{H}$ is a constant of motion (as the Hamiltonian (17) does not explicitly depend on τ) and using Equations (12) and (21), the condition (23) with $s = 1$ (the thruster is on to start the orbital transfer) gives

$$\mathcal{H}(\tau_0) = \lambda_v(\tau_0)\,\beta = 1 \tag{24}$$

and the initial value λ_v is

$$\lambda_v(\tau_0) = \frac{1}{\beta} \tag{25}$$

Finally, the transversality condition gives an additional equation related to the terminal constraint (recall that the transverse component of the dimensionless spacecraft velocity is $1/\rho$), that is

$$\mathcal{E}(\tau_f) = \frac{v_f^2}{2} + \frac{1}{2\,\rho_f^2} - \frac{1}{\rho_f} = \mathcal{E}_f \tag{26}$$

where $v_f = v(\tau_f)$, $\rho_f = \rho(\tau_f)$, and $\mathcal{E}_f$ is the final value of the orbital energy given by Equation (15). Note that Equation (26) can be rewritten in standard form as

$$\chi \triangleq \frac{v_f^2}{2} + \frac{1}{2\,\rho_f^2} - \frac{1}{\rho_f} - \mathcal{E}_f = 0 \tag{27}$$

so that the transversality condition gives

$$\rho_f^3\, v_f\, \lambda_\rho(\tau_f) = \left(\rho_f - 1\right) \lambda_v(\tau_f) \tag{28}$$

Using the Pontryagin's maximum principle, the control function $s = s(\tau)$ is obtained by maximizing, at any time τ, the portion of the Hamiltonian that explicitly depends on the control s, that is

$$\mathcal{H}' \triangleq \lambda_v\, \frac{s\,\beta}{\rho} \tag{29}$$

Since ρ and β are both positive parameters, the maximization of $\mathcal{H}'$ gives a bang-bang control law

$$s = \frac{\operatorname{sign}(\lambda_v) + 1}{2} \tag{30}$$

where $\operatorname{sign}(\square)$ is the signum function. In other terms, the costate λ_v plays the role of a switching function in determining the value of s. Note that the characteristics of the target orbit appear in Equation (27) through the orbital energy $\mathcal{E}_f$ defined in Equation (15).

The initial value of the costate λ_ρ and the optimal flight time τ_f are solutions of a two-point boundary value problem (TPBVP) in which the two final constraints are given by Equations (27) and (28). The TPBVP has been solved, with an absolute error less than 10^{-8}, through a hybrid numerical technique that uses gradient-based and stochastic methods. Finally, the spacecraft nonlinear equations of motion have been numerically integrated with a variable order Adams-Bashforth-Moulton PECE solver, with absolute and relative errors equal to 10^{-10}. The numerical results are presented in the next section.

3. Numerical Simulations

The previous optimization procedure has been implemented to simulate the optimal circle-to-ellipse transfer of a Sun-facing E-sail for twenty different mission scenarios, corresponding to all possible combinations of $e_f \in \{0.1, 0.2, 0.3, 0.4, 0.5\}$ and $\beta \in \{0.2, 0.3, 0.4, 0.5\}$.

The main simulation results are reported in Figure 2, which, in its left-hand side, shows the function $\tau_f = \tau_f(e_f, \beta)$ obtained with a two-dimensional interpolation procedure of the numerical results (black circles), while the right-hand side of the figure illustrates the level curves of the same function.

The main characteristics of the rendez-vous point, that is, $\{\rho_f, \theta_f, v_f, \nu_f\}$, are summarized in Figure 3 as a function of the design parameters $\{e_f, \beta\}$, where $\nu_f \in [0, 2\pi]$ rad is the spacecraft true anomaly on the target orbit, calculated with the conic polar equation in dimensionless form, that is

$$\nu_f = \arccos\left[\frac{1}{e_f}\left(\frac{1}{\rho_f} - 1\right)\right] \quad \text{with} \quad \nu_f \in \begin{cases} [0, \pi]\ \text{rad} & \text{if} \quad v_f \geq 0 \\ (\pi, 2\pi]\ \text{rad} & \text{if} \quad v_f < 0 \end{cases} \tag{31}$$

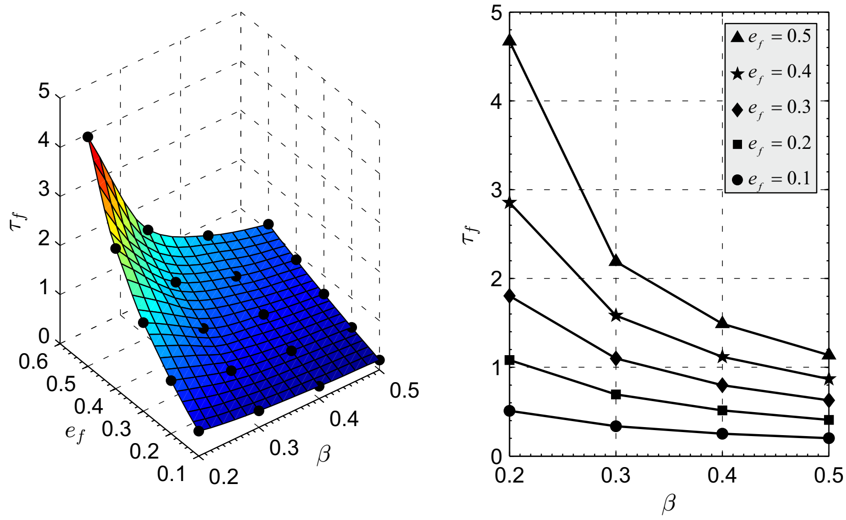

Figure 2. Minimum flight time τ_f as a function of e_f and β.

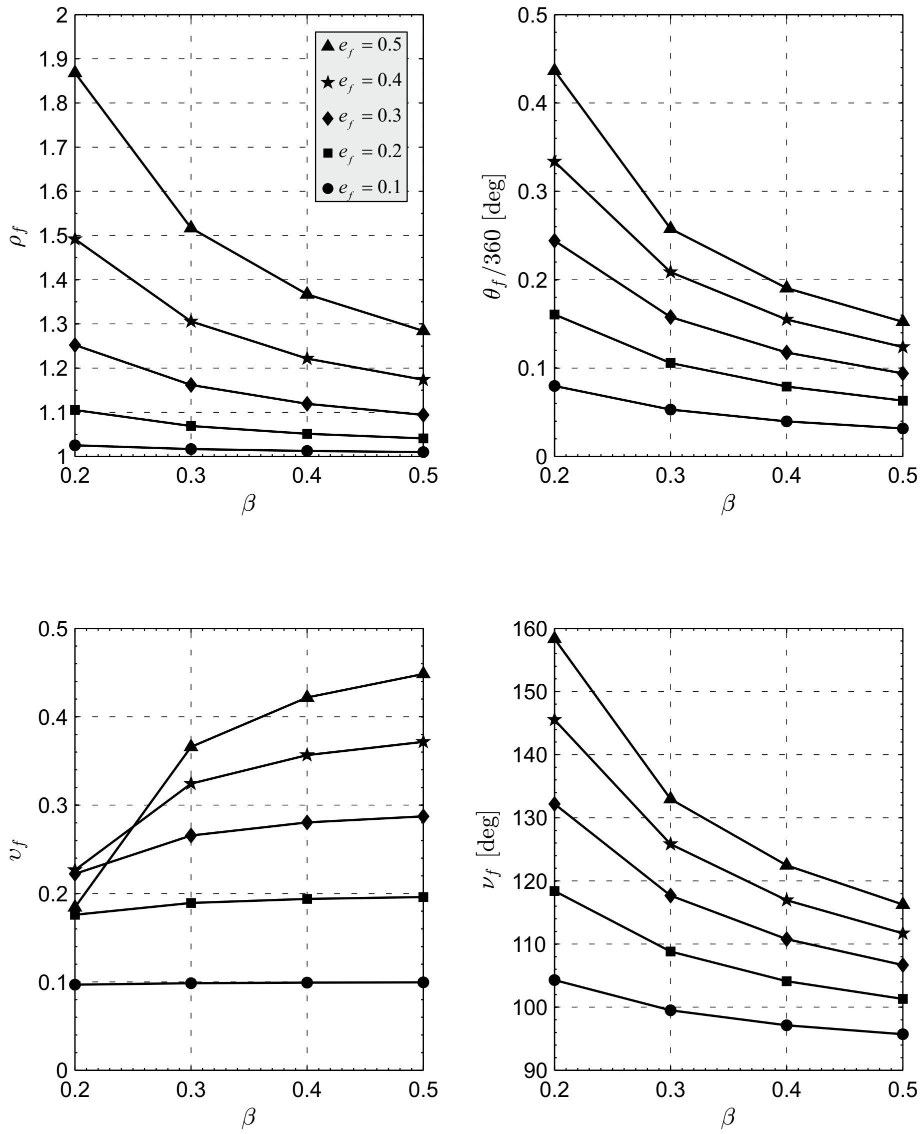

Figure 3. Characteristics of the rendez-vous point as a function of e_f and β.

Finally, Figure 4 reports the semimajor axis a_f and apse line rotation angle ω_f (see Figure 1) of the elliptic target orbit.

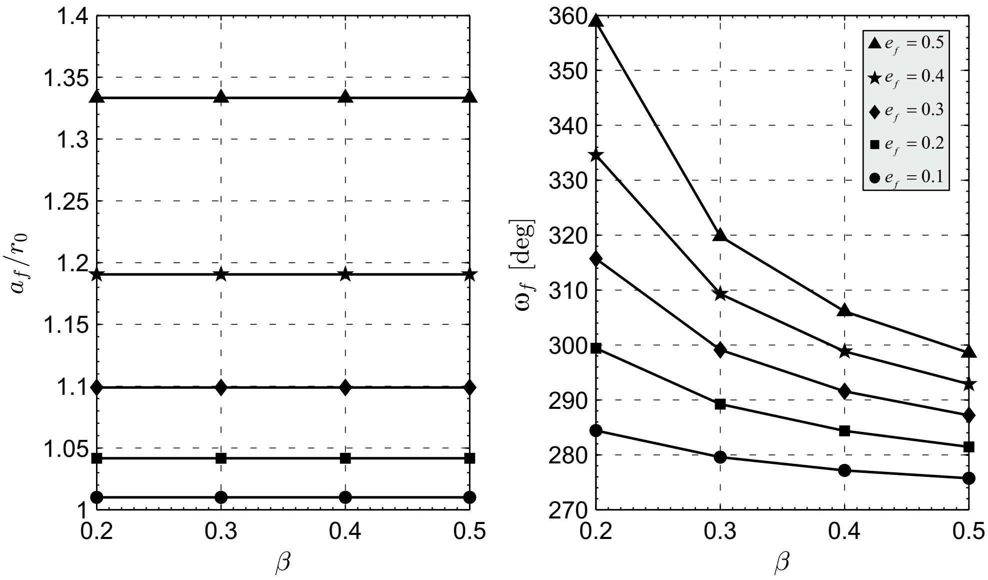

Figure 4. Geometric characteristics of target elliptic orbit as a function of e_f and β.

The data of Figures 2–4 are useful for obtaining a quick estimate of the overall transfer mission performance in a generic problem, because their values are independent of the radius r_0 of the circular parking.

The twenty analyzed mission scenarios, that is, the optimal transfer trajectories that are representative of the two design parameters ranging in the intervals $e_f \in [0.1, 0.5]$ and $\beta \in [0.2, 0.5]$, are characterized by the absence of coasting arcs in the transfer trajectory, which is completed in less than one full revolution around the Sun. This aspect is evident in Figures 5 and 6, which show the results of the numerical simulation for the case of $e_f = 0.3$ and $\beta = 0.2$, while Figure 7 shows the optimal transfer trajectory for three sets of design parameters.

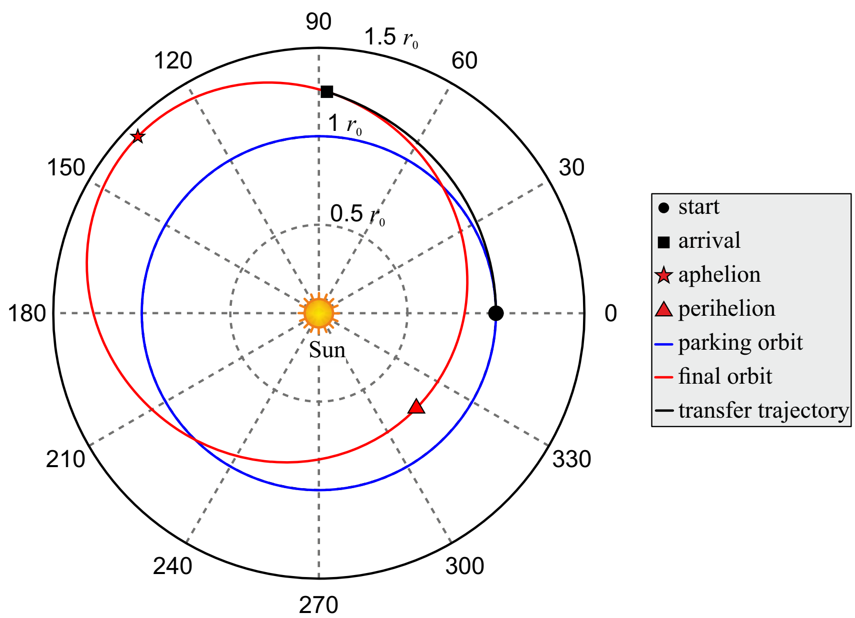

Figure 5. Optimal transfer trajectory when $e_f = 0.3$ and $\beta = 0.2$.

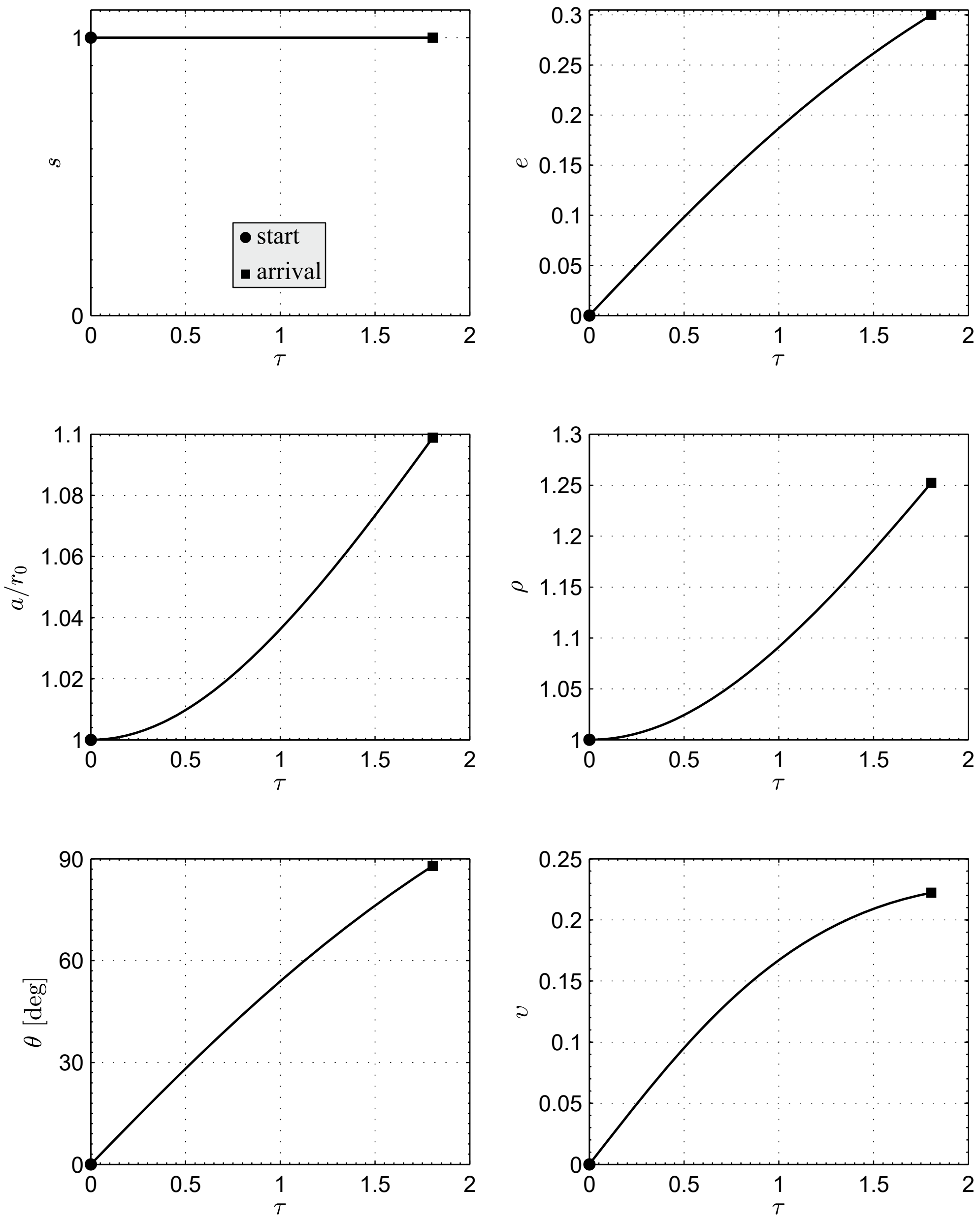

Figure 6. Optimal τ-variation of the spacecraft states when $e_f = 0.3$ and $\beta = 0.2$.

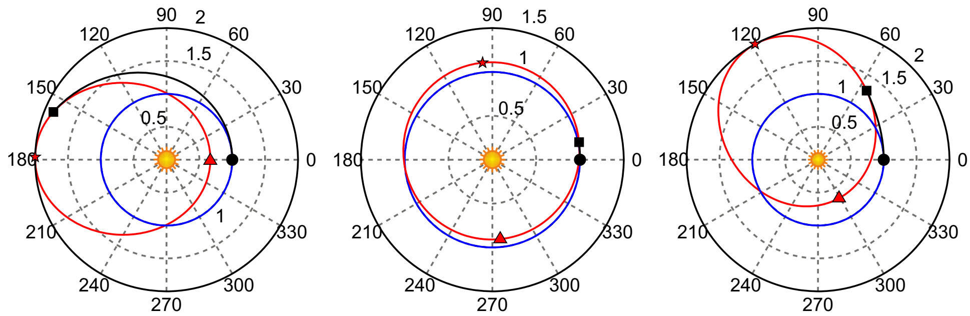

(**a**) $\beta = 0.2$ and $e_f = 0.5$. (**b**) $\beta = 0.5$ and $e_f = 0.1$. (**c**) $\beta = 0.5$ and $e_f = 0.5$.

Figure 7. Optimal transfer trajectory for some set of design parameters.

A more involved transfer trajectory, with a coasting arc, results when β is sufficiently small. For example, Figures 8 and 9 show the numerical simulations for $e_f = 0.3$ and

$\beta = 0.1$. In this case, the spacecraft completes a full revolution around the Sun before reaching the final orbit, and a coating arc appears in the time range $\tau \in [2, 6]$.

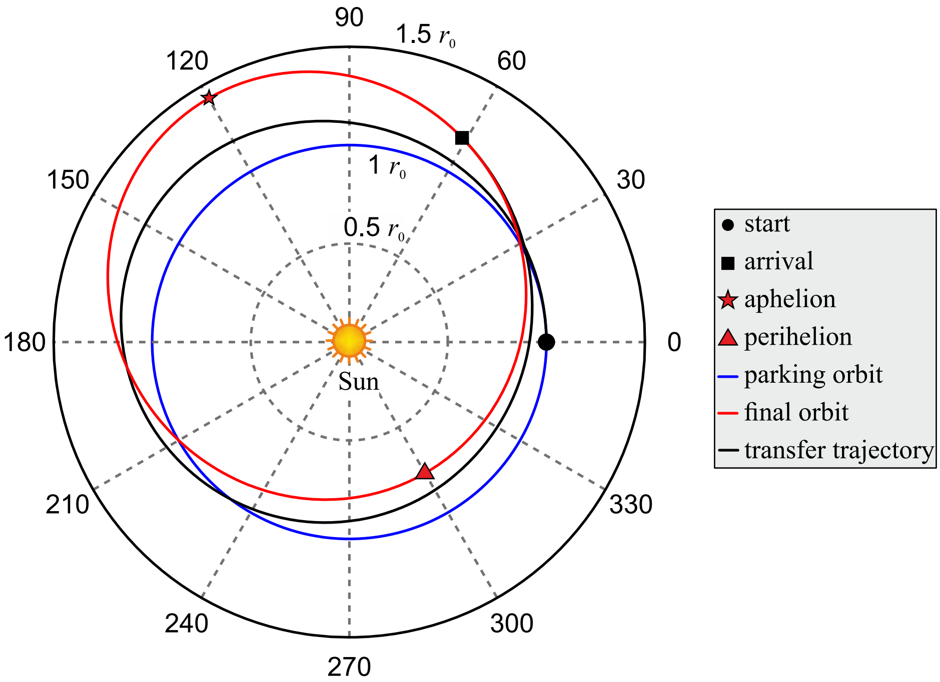

Figure 8. Optimal transfer trajectory when $e_f = 0.3$ and $\beta = 0.1$.

The proposed procedure can be used in the study of an interplanetary mission application, as discussed in the next section.

3.1. Mission Application

Consider an interplanetary mission scenario in which the Earth and the target planet orbit are assumed to be coplanar and circular. Starting from a heliocentric orbit of radius $r_0 = 1\,\mathrm{au}$, which models a spacecraft deployment along a parabolic escape orbit relative to the Earth, the Sun-facing E-sail is used to insert the vehicle into an elliptic target orbit, whose aphelion (or perihelion) lies on the circular orbit of the target (inner or outer) planet. In this case, the Sun's gravitational acceleration along the parking orbit is $\mu_\odot / r_0^2 \simeq 5.93\,\mathrm{mm/s^2}$, so that the maximum propulsive acceleration can be written as

$$\max \|\boldsymbol{a}_p\| \simeq \beta \times 5.93\,\mathrm{mm/s^2} \quad \text{when} \quad r = r_0 \triangleq 1\,\mathrm{au} \tag{32}$$

while the semimajor axis of the elliptic target orbit, as a function of its eccentricity e_f, is

$$a_f = \frac{1\,\mathrm{au}}{1 - e_f^2} \tag{33}$$

Finally, the perihelion and aphelion radius are, respectively

$$r_p = \frac{1\,\mathrm{au}}{1 + e_f} \tag{34}$$

$$r_a = \frac{1\,\mathrm{au}}{1 - e_f} \tag{35}$$

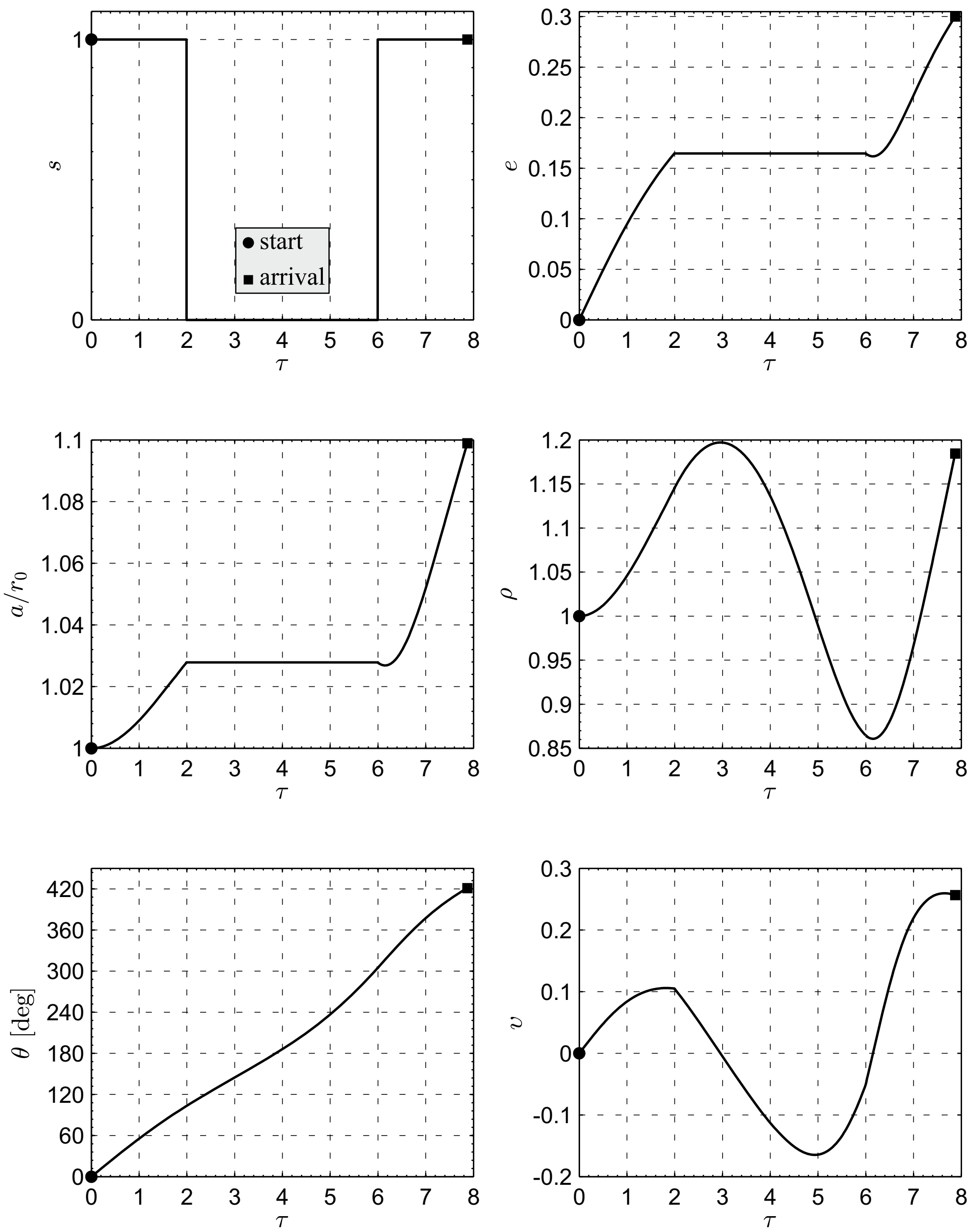

Figure 9. Optimal τ-variation of the spacecraft states when $e_f = 0.3$ and $\beta = 0.1$.

3.1.1. Mars Case

Consider first a transfer towards Mars, where the planet orbit is approximated as a circular trajectory of radius $r = r_{♂} \triangleq 1.524\,\text{au}$. In this case, assuming that the aphelion radius r_a of the elliptic target orbit is equal to $r_{♂}$, Equation (35) gives the value of the (target) eccentricity e_f, that is

$$e_f = 1 - \frac{1\,\text{au}}{r_{♂}} \simeq 0.3438 \tag{36}$$

Using the eccentricity from the last equation and considering an E-sail with $\beta \in \{0.2, 0.3, 0.4, 0.5\}$, the proposed optimization procedure gives the results summarized in Figure 10. The figure shows that an elliptic orbit with an aphelion radius equal to the heliocentric distance of Mars can be reached with a flight time on the order of one hundred days.

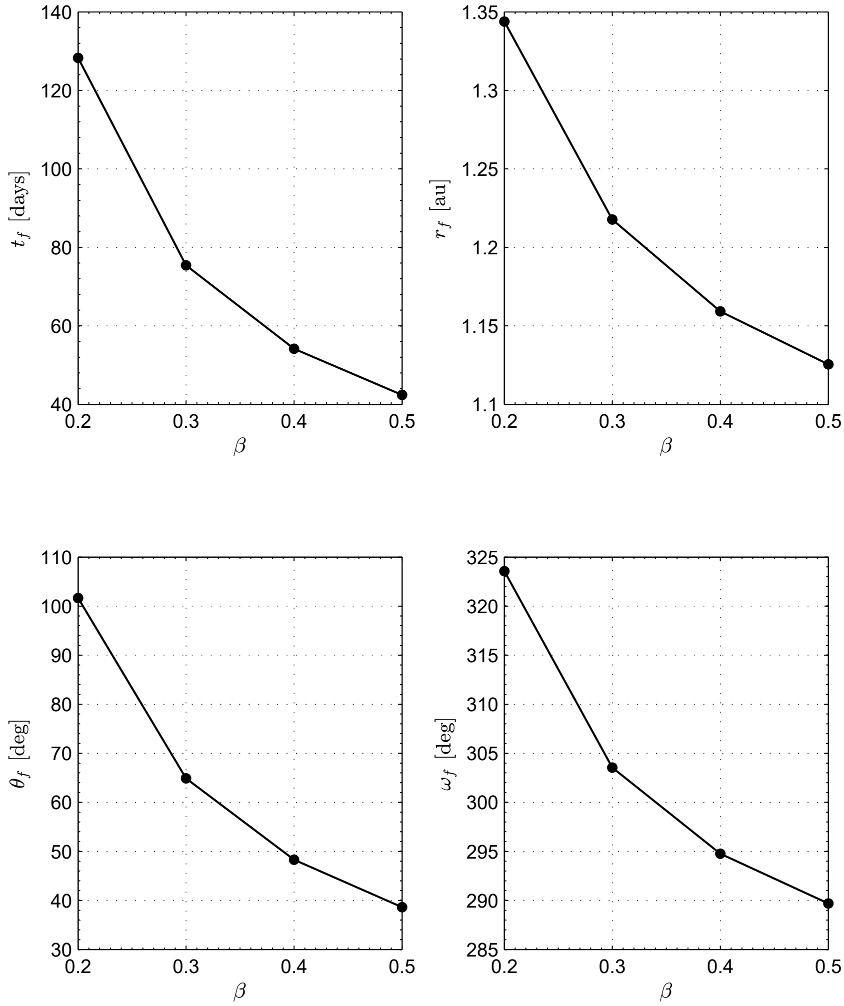

Figure 10. Optimal transfer performances in a Mars-based mission scenario ($e_f = 0.3438$) as a function of β.

For example, assuming $\beta = 0.3$, which corresponds to a maximum propulsive acceleration of about $1.8\,\text{mm/s}^2$ at 1 au, the optimal transfer trajectory and the transfer orbit characteristics are reported in Figures 11 and 12, respectively.

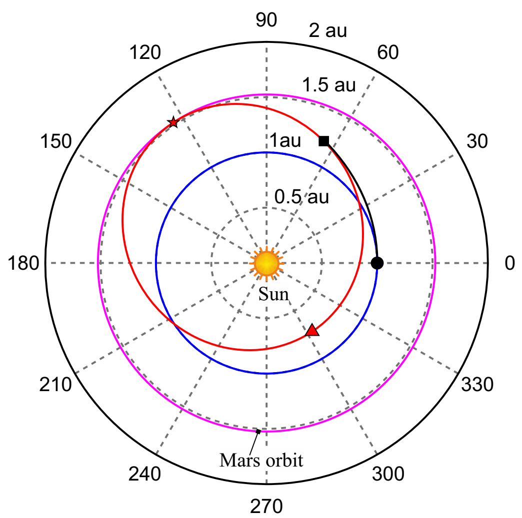

Figure 11. Optimal transfer trajectory in a Mars-based mission scenario with $e_f = 0.3438$ and $\beta = 0.3$.

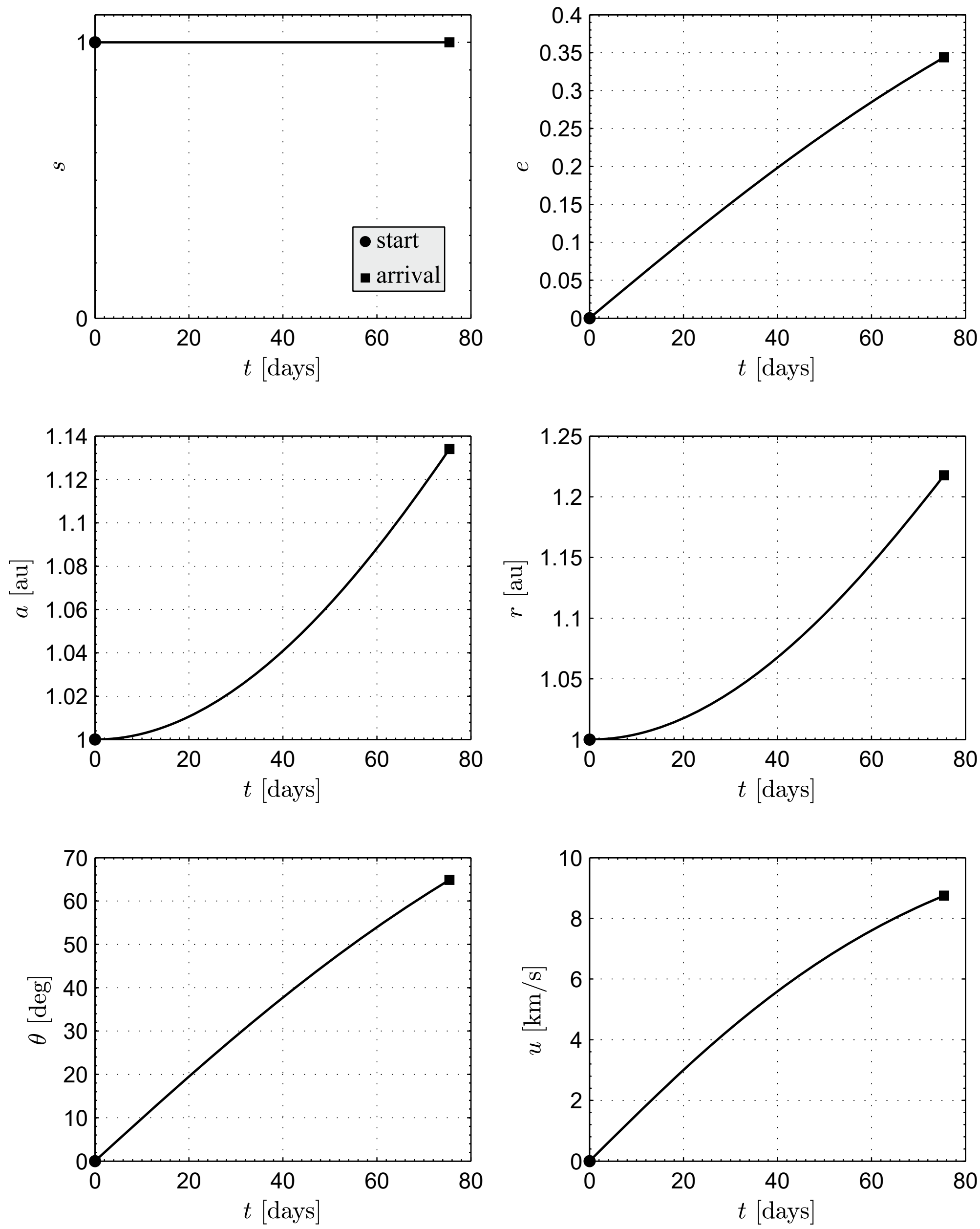

Figure 12. Transfer trajectory characteristics in a Mars-based mission scenario with $e_f = 0.3438$ and $\beta = 0.3$.

3.1.2. Venus case

Consider now a circular heliocentric orbit of radius $r = r_♀ = 0.723\,\mathrm{au}$, that is, a scenario that models a transfer towards Venus. In that case, from Equation (34), the eccentricity of the target orbit is obtained by enforcing the constraint $r_p = r_♀$, and the result is

$$e_f = \frac{1\,\mathrm{au}}{r_♀} - 1 \simeq 0.3831 \tag{37}$$

Using the usual range of variation of $\beta \in \{0.2, 0.3, 0.4, 0.5\}$, the simulation results are summarized in Figure 13, while Figures 14 and 15 give the transfer characteristics when $\beta = 0.3$.

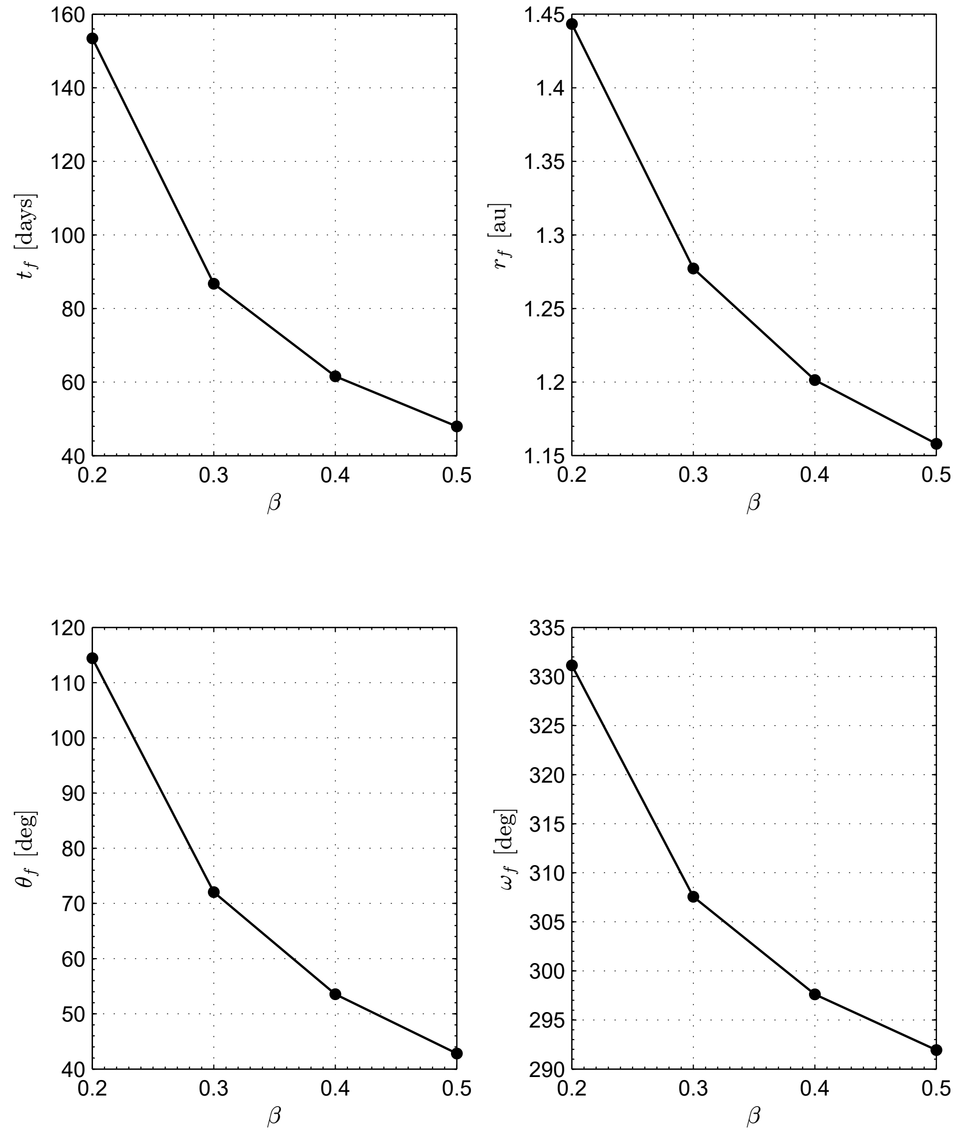

Figure 13. Optimal transfer performances in a Venus-based mission scenario ($e_f = 0.3831$) as a function of β.

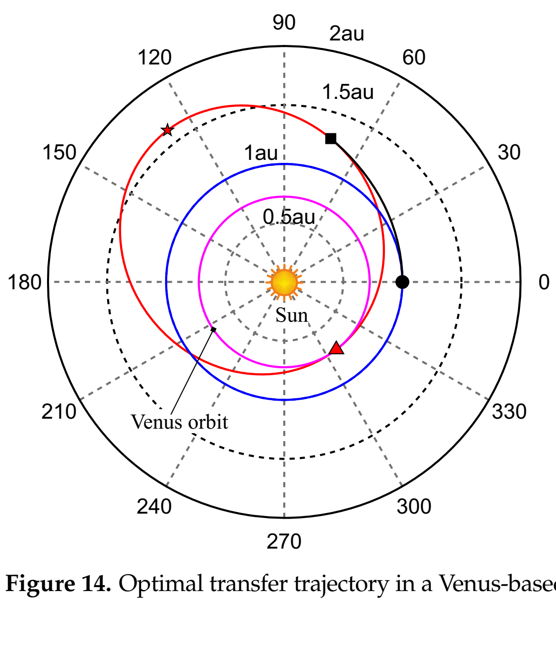

Figure 14. Optimal transfer trajectory in a Venus-based mission scenario with $e_f = 0.3831$ and $\beta = 0.3$.

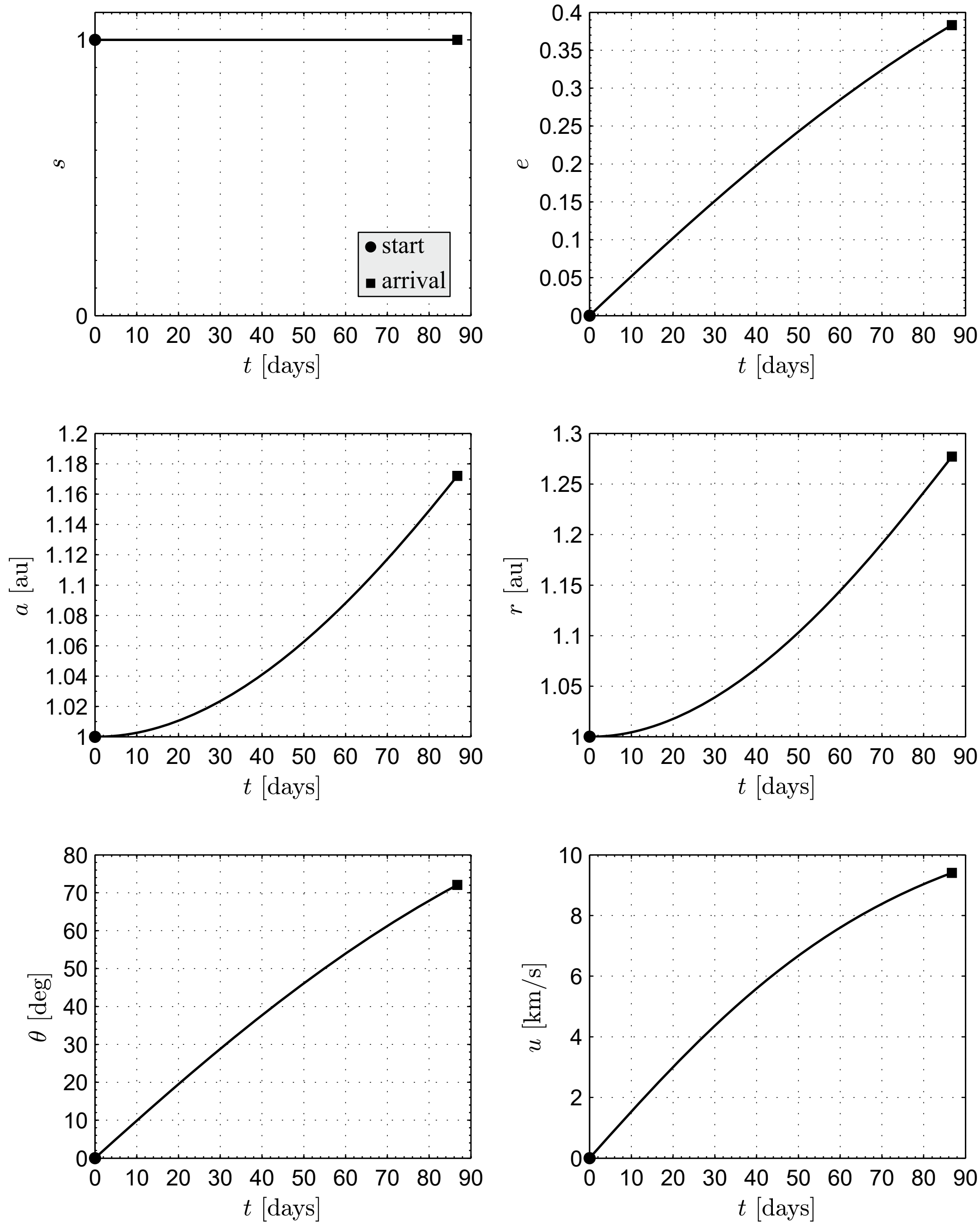

Figure 15. Transfer trajectory characteristics in a Venus-based mission scenario with $e_f = 0.3831$ and $\beta = 0.3$.

3.1.3. Jupiter Case

The final mission case refers to a more challenging transfer towards Jupiter, with a maximum propulsive acceleration of $1\,\mathrm{mm/s^2}$, which, according to Equation (32), corresponds to an E-sail with $\beta \simeq 0.1686$. In this case, we assume a circular Jupiter orbit of radius $r = r_{♃} = 5.2\,\mathrm{au}$, so that Equation (35) provides $e_f = 0.8077$ as target eccentricity. This case is characterized by a large value of the target eccentricity and a relatively small value of the E-sail propulsive acceleration. In fact, the optimal transfer trajectory obtained with the proposed approach is more involved and contains a single coasting arc, as shown in Figure 16.

In this case, the transfer trajectory characteristics are summarized in Figure 17.

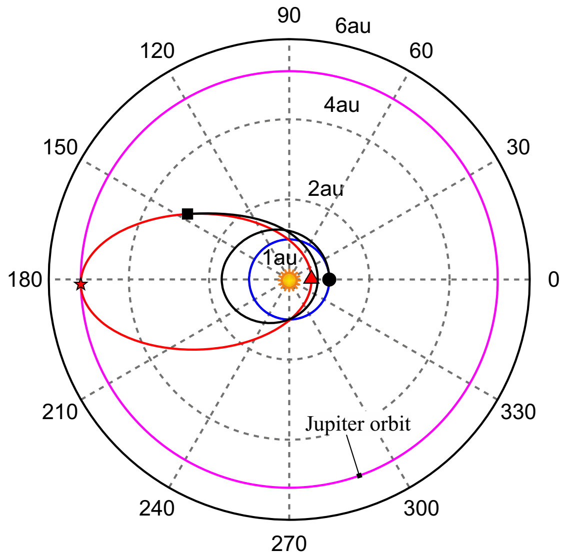

Figure 16. Optimal transfer trajectory in a Jupiter-based mission scenario with $e_f = 0.8077$ and $\beta = 0.1686$.

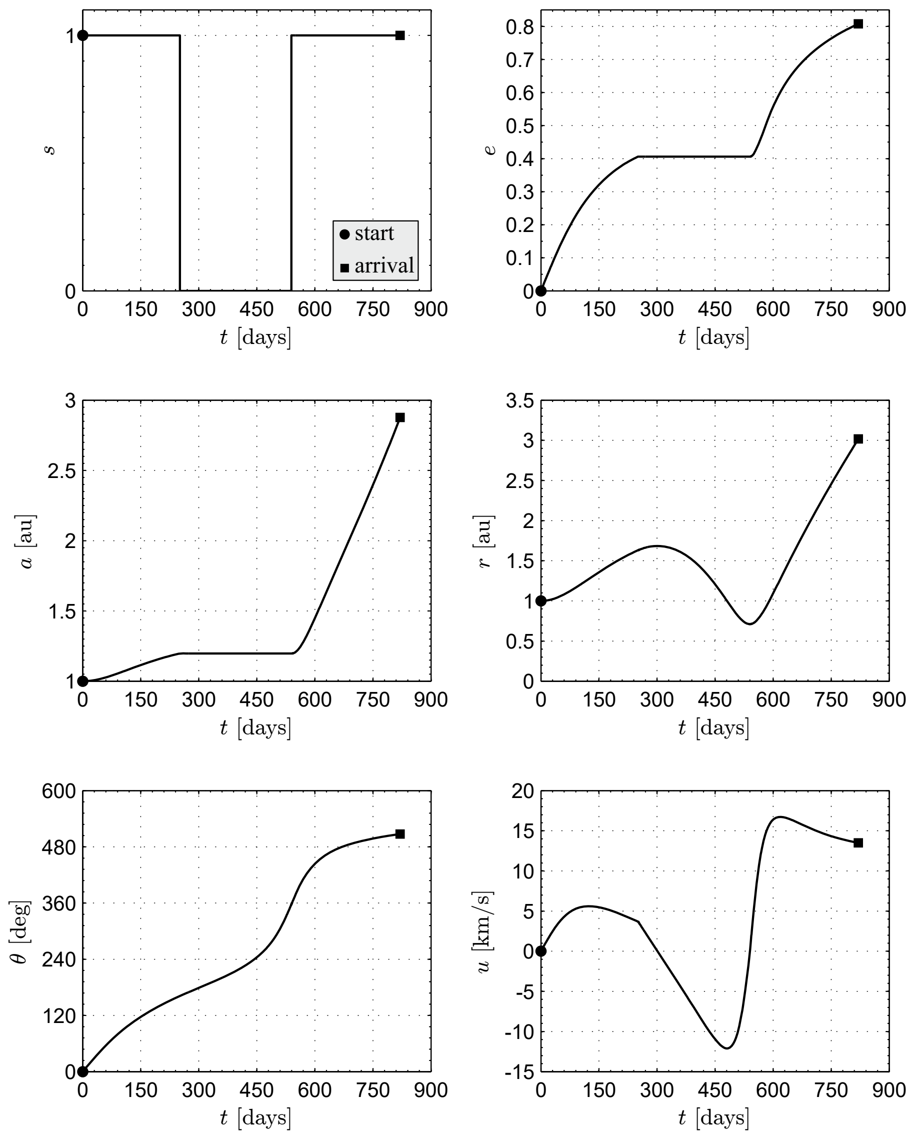

Figure 17. Transfer trajectory characteristics in a Jupiter-based mission scenario with $e_f = 0.8077$ and $\beta = 0.1686$.

4. Conclusions

This paper has analyzed the transfer performance of a spacecraft propelled by an Electric Solar Wind Sail with a Sun-facing attitude in a two-dimensional circle-to-ellipse mission scenario. With the introduction of a suitable set of dimensionless spacecraft states, the proposed approach allows the transfer performance of the spacecraft to be evaluated as a function of two parameters only, that is, the final value of the orbital eccentricity and the sail propulsive performance. To that end, the paper presents a set of graphs that can be used to obtain a quick estimate of the minimum flight time and the characteristics of the final orbit without the need of any numerical simulation. The paper also shows a simplified mathematical model for the spacecraft trajectory optimization, which is able to numerically solve the two-point boundary value problem associated with the optimization procedure in a simple and effective way. The potential extensions of this work are related to the analysis of circle-to-ellipse transfers of the Sun-facing Electric Solar Wind Sail in the presence of an intermediate gravity assist maneuver. In that case the flyby could be used, for example, to change the value of the osculating orbit semilatus rectum, thus increasing the degrees of freedom in the design of the final orbit shape.

Author Contributions: Conceptualization, A.A.Q.; methodology, A.A.Q.; software, A.A.Q.; writing—original draft preparation, A.A.Q., M.B., L.N.; writing—review and editing, G.M. All authors have read and agreed to the published version of the manuscript.

Funding: This work is supported by the University of Pisa, Progetti di Ricerca di Ateneo (Grant no. PRA_2022_1).

Institutional Review Board Statement: Not applicable.

Informed Consent Statement: Not applicable.

Data Availability Statement: Not applicable.

Conflicts of Interest: The authors declare no conflict of interest.

Abbreviations

a	osculating orbit semimajor axis [au]
$\boldsymbol{a}_p$	propulsive acceleration vector [mm/s^2]
e	osculating orbit eccentricity
E	specific orbital energy [km^2/s^2]
$\mathcal{E}$	dimensionless specific orbital energy
h	orbital specific angular momentum magnitude [km^2/s]
$\mathcal{H}$	dimensionless Hamiltonian function
$\hat{\boldsymbol{\imath}}_r$	radial unit vector
$\hat{\boldsymbol{\imath}}_\theta$	transverse unit vector
J	dimensionless performance index
O	Sun's center of mass
p	semilatus rectum [au]
r	Sun-spacecraft radial distance [au]
s	dimensionless switching parameter
t	time [days]
$\mathcal{T}$	polar reference frame
u	radial component of the spacecraft velocity [km/s]
β	dimensionless reference propulsive acceleration magnitude
θ	polar angle [rad]
λ_ρ	dimensionless variable adjoint to ρ
λ_v	dimensionless variable adjoint to v
λ_θ	dimensionless variable adjoint to θ
$\mu_\odot$	Sun's gravitational parameter [km^3/s^2]
ρ	dimensionless radial distance
τ	dimensionless time
v	dimensionless radial velocity

χ	final dimensionless constraint
ω	osculating orbit apse line rotation angle [rad]
Subscripts	
0	initial, parking orbit
a	aphelion
f	final, target orbit
♃	Jupiter
♂	Mars
p	perihelion
♀	Venus

References

1. Bassetto, M.; Niccolai, L.; Quarta, A.A.; Mengali, G. A comprehensive review of Electric Solar Wind Sail concept and its applications. *Prog. Aerosp. Sci.* **2022**, *128*, 100768. [CrossRef]
2. Janhunen, P. Electric sail for spacecraft propulsion. *J. Propuls. Power* **2004**, *20*, 763–764. [CrossRef]
3. Janhunen, P.; Lebreton, J.P.; Merikallio, S.; Paton, M.; Mengali, G.; Quarta, A.A. Fast E-sail Uranus entry probe mission. *Planet. Space Sci.* **2014**, *104*, 141–146. [CrossRef]
4. Mengali, G.; Quarta, A.A.; Janhunen, P. Considerations of electric sailcraft trajectory design. *J. Br. Interplanet. Soc.* **2008**, *61*, 326–329.
5. Quarta, A.A.; Mengali, G. Electric sail mission analysis for outer solar system exploration. *J. Guid. Control Dyn.* **2010**, *33*, 740–755. [CrossRef]
6. Sanchez-Torres, A. Propulsive force in electric solar sails for missions in the heliosphere. *IEEE Trans. Plasma Sci.* **2019**, *47*, 1657–1662. [CrossRef]
7. Bassetto, M.; Quarta, A.A.; Mengali, G. Locally-optimal electric sail transfer. *Proc. Inst. Mech. Eng. Part G J. Aerosp. Eng.* **2019**, *233*, 166–179. [CrossRef]
8. Mengali, G.; Quarta, A.A. Trajectory analysis and optimization of Hesperides mission. *Universe* **2022**, *8*. 364. [CrossRef]
9. Matloff, G.L. The Solar-Electric Sail: Application to Interstellar Migration and Consequences for SETI. *Universe* **2022**, *8*, 252. [CrossRef]
10. Niccolai, L.; Anderlini, A.; Mengali, G.; Quarta, A.A. Electric sail displaced orbit control with solar wind uncertainties. *Acta Astronaut.* **2019**, *162*, 563–573. [CrossRef]
11. Niccolai, L.; Caruso, A.; Quarta, A.A.; Mengali, G. Artificial collinear Lagrangian point maintenance with electric solar wind sail. *IEEE TRansactions Aerosp. Electron. Syst.* **2020**, *56*, 4467–4477. [CrossRef]
12. Merikallio, S.; Janhunen, P. Moving an asteroid with electric solar wind sail. *Astrophys. Space Sci. Trans.* **2010**, *6*, 41–48. [CrossRef]
13. Yamaguchi, K.; Yamakawa, H. Electric solar wind sail kinetic energy impactor for Near Earth Asteroid deflection mission. *J. Astronaut. Sci.* **2016**, *63*, 1–22. [CrossRef]
14. Sanchez-Torres, A. Propulsive force in an electric solar sail for outer planet missions. *IEEE Trans. Plasma Sci.* **2015**, *43*, 3130–3135. [CrossRef]
15. Huo, M.Y.; Mengali, G.; Quarta, A.A. Optimal planetary rendezvous with an electric sail. *Aircr. Eng. Aerosp. Technol.* **2016**, *88*, 515–522. [CrossRef]
16. Quarta, A.A.; Mengali, G.; Janhunen, P. Electric sail option for cometary rendezvous. *Acta Astronaut.* **2016**, *127*, 684–692. [CrossRef]
17. Slavinskis, A.; Janhunen, P.; Toivanen, P.; Muinonen, K.; Penttilä, A.; Granvik, M.; Kohout, T.; Gritsevich, M.; Pajusalu, M.; Sunter, I.; et al. Nanospacecraft fleet for multi-asteroid touring with electric solar wind sails. In Proceedings of the IEEE Aerospace Conference Proceedings, Big Sky, MT, USA, 3–10 March 2018; pp. 1–20. [CrossRef]
18. Huo, M.Y.; Zhang, G.; Qi, N.; Liu, Y.; Shi, X. Initial trajectory design of electric solar wind sail based on finite Fourier series shape-based method. *IEEE Trans. Aerosp. Electron. Syst.* **2019**, *55*, 3674–3683. [CrossRef]
19. Huo, M.Y.; Mengali, G.; Quarta, A.A. Electric sail thrust model from a geometrical perspective. *J. Guid. Control Dyn.* **2018**, *41*, 735–741. [CrossRef]
20. Li, G.; Zhu, Z.H.; Du, C.; Meguid, S.A. Characteristics of coupled orbital-attitude dynamics of flexible electric solar wind sail. *Acta Astronaut.* **2019**, *159*, 593–608. [CrossRef]
21. Zhao, C.; Huo, M.Y.; Qi, J.; Cao, S.; Zhu, D.; Sun, L.; Sun, H.; Qi, N. Coupled attitude-vibration analysis of an E-sail using absolute nodal coordinate formulation. *Astrodynamics* **2020**, *4*, 249–263. [CrossRef]
22. Du, C.; Zhu, Z.H.; Li, G. Analysis of thrust-induced sail plane coning and attitude motion of electric sail. *Acta Astronaut.* **2021**, *178*, 129–142. [CrossRef]
23. Du, C.; Zhu, Z.H.; Kang, J. Attitude control and stability analysis of electric sail. *IEEE Trans. Aerosp. Electron. Syst.* **2022**. [CrossRef]
24. Bassetto, M.; Mengali, G.; Quarta, A.A. Thrust and torque vector characteristics of axially-symmetric E-sail. *Acta Astronaut.* **2018**, *146*, 134–143. [CrossRef]

25. Bassetto, M.; Mengali, G.; Quarta, A.A. Attitude dynamics of an electric sail model with a realistic shape. *Acta Astronaut.* **2019**, *159*, 250–257. [CrossRef]
26. Bassetto, M.; Mengali, G.; Quarta, A.A. Stability and control of spinning E-sail in heliostationary orbit. *J. Guid. Control Dyn.* **2019**, *42*, 425–431. [CrossRef]
27. Bassetto, M.; Mengali, G.; Quarta, A.A. E-sail attitude control with tether voltage modulation. *Acta Astronaut.* **2020**, *166*, 350–357. [CrossRef]
28. Mengali, G.; Quarta, A.A.; Aliasi, G. A graphical approach to electric sail mission design with radial thrust. *Acta Astronaut.* **2013**, *82*, 197–208. [CrossRef]
29. Quarta, A.A.; Mengali, G. Analysis of electric sail heliocentric motion under radial thrust. *J. Guid. Control Dyn.* **2016**, *39*, 1431–1435. [CrossRef]
30. Bassetto, M.; Quarta, A.A.; Mengali, G.; Cipolla, V. Spiral trajectories induced by radial thrust with applications to generalized sails. *Astrodynamics* **2020**, *5*, 121–137. [CrossRef]
31. Bassetto, M.; Boni, L.; Mengali, G.; Quarta, A.A. Electric sail phasing maneuvers with radial thrust. *Acta Astronaut.* **2021**, *179*, 99–104. [CrossRef]
32. Fu, B.; Sperber, E.; Eke, F. Solar sail technology—A state of the art review. *Prog. Aerosp. Sci.* **2016**, *86*, 1–19. [CrossRef]
33. Bovesecchi, G.; Corasaniti, S.; Costanza, G.; Tata, M.E. A novel self-deployable solar sail system activated by shape memory alloys. *Aerospace* **2019**, *6*, 78. [CrossRef]
34. Zhang, F.; Gong, S.; Baoyin, H. Three-axes attitude control of solar sail based on shape variation of booms. *Aerospace* **2021**, *8*, 198. [CrossRef]
35. Zou, J.; Li, D.; Wang, J.; Yu, Y. Experimental study of measuring the wrinkle of solar sails. *Aerospace* **2022**, *9*, 289. [CrossRef]
36. McInnes, C.R. Orbits in a generalized two-body problem. *J. Guid. Control Dyn.* **2003**, *26*, 743–749. [CrossRef]
37. Niccolai, L.; Bassetto, M.; Quarta, A.A.; Mengali, G. A review of Smart Dust architecture, dynamics, and mission applications. *Prog. Aerosp. Sci.* **2019**, *106*, 1–14. [CrossRef]
38. Yamakawa, H. Optimal radially accelerated interplanetary trajectories. *J. Spacecr. Rocket.* **2006**, *43*, 116–120. [CrossRef]
39. Bassetto, M.; Quarta, A.A.; Mengali, G.; Cipolla, V. Trajectory analysis of a Sun-facing solar sail with optical degradation. *J. Guid. Control Dyn.* **2020**, *43*, 1727–1732. [CrossRef]
40. McInnes, C.R. Solar sail mission applications for non-Keplerian orbits. *Acta Astronaut.* **1999**, *45*, 567–575. [CrossRef]
41. Aliasi, G.; Mengali, G.; Quarta, A.A. Artificial equilibrium points for a generalized sail in the elliptic restricted three-body problem. *Celest. Mech. Dyn. Astron.* **2012**, *114*, 181–200. [CrossRef]
42. Morante, D.; Sanjurjo Rivo, M.; Soler, M. A Survey on Low-Thrust Trajectory Optimization Approaches. *Aerospace* **2021**, *8*, 88. [CrossRef]
43. Vepa, R.; Shaheed, M.H. Optimal Trajectory Synthesis for Spacecraft Asteroid Rendezvous. *Symmetry* **2021**, *13*, 1403. [CrossRef]
44. Shi, J.; Wang, J.; Su, L.; Ma, Z.; Chen, H. A Neural Network Warm-Started Indirect Trajectory Optimization Method. *Aerospace* **2022**, *9*, 435. [CrossRef]
45. Janhunen, P.; Quarta, A.A.; Mengali, G. Electric solar wind sail mass budget model. *Geosci. Instrum. Methods Data Syst.* **2013**, *2*, 85–95. [CrossRef]